Effect of cryorolling on microstructure and mechanical properties of a peak-aged AA6082 extrusion

Zebing Xu [a], Manping Liu [b,*], Zhihong Jia [c], Hans J. Roven [a,*]

[a] NTNU, Norwegian University of Science and Technology, Department of Materials Science and Engineering, 7491 Trondheim, Norway

[b] School of Materials Science and Engineering, Jiangsu University, Zhenjiang 212013, China

[c] College of Materials Science and Engineering, Chongqing University, Chongqing 400044, China

* Corresponding authors. *E-mail addresses*: manpingliu@ujs.edu.cn (M.P. Liu), hans.j.roven@material.ntnu.no (H.J. Roven)

Abstract: Peak-aged AA6082 flat extrusions were cryorolled at liquid nitrogen temperature to three different thickness reductions, the reductions were 21%, 42% and 85%, respectively. For comparison, an identical extrusion was rolled at room temperature to a reduction of 85%. The microstructure and plastic deformation behaviors of the initial as well as the rolled materials were studied by means of electron microscopy and tensile tests at room temperature. The initial material showed fibrous grain structure. After cryorolling to 21% thickness reduction, grains in the alloy were further elongated. In addition, microbands were detected in some grains, while other grains were microband-free. More detailed information was obtained in the sample after 42% thickness reduction. Here, numerous microbands aligned along slip planes with the highest resolved shear stress, leading to the formation of new low angle subgrains and high angle grains. In the case of microband-free grains, multiple slip systems were activated concurrently due to similar and low Schmid factors, hence producing homogeneous deformation within these grains. A cryorolling strain of 85% produced a hierarchical microstructure in the materials volume, consisting of nano- and ultrafine grains with size < 100 nm coexisted with micro-sized grains. The development of hierarchical

microstructure could be considered as a consequence of the intersection between families of microbands. As a result, both the strength and uniform elongation of the severely cryorolled alloy, i.e. 85% thickness reduction, are more superior to rest of rolled alloys. Therefore, this study revealed that a simple processing procedure, i.e., cryorolling, can be utilized to tailor for desired properties in favor of both strength and ductility aluminum alloy.

Keywords: Peak-aged AA6082 alloy; Cryorolling; Microbands; Hierarchical microstructure; Mechanical properties

1. Introduction

Aluminum alloys are widely used for fabricating structural components in the automobile and aerospace industries because of their high strength-to-weight ratio, good formability and high corrosion resistance [1-3]. One of the powerful routes by which Al alloys can gain superior mechanical properties is grain refinement [4]. Due to the formation of ultrafine grained (UFG) structures, a significant enhancement in mechanical properties such as hardness, toughness, ductility and strength can be achieved. It is well known that severe plastic deformation (SPD) technique, such as equal channel angular pressing (ECAP) [5], high pressure torsion (HPT) [6] and dynamic plastic deformation (DPD) [7] etc., are viable routes to produce UFG materials from their bulk counterparts. However, what is frustrating to researchers is that, only relatively small sized semi-products can be produced by these techniques. The up-scaling of processes is difficult, and their industry applications are therefore restrained.

To overcome these difficulties, conventional rolling at cryogenic temperature, i.e., cryorolling, has been suggested. The latter is a simple low-temperature process that required a relatively low force to induce severe strains in materials. As a matter of fact, cryorolling has

been identified as one of the potential processes to produce nanostructured or ultrafine-grained materials at large scale [8]. Recently, the effect of cryorolling on the microstructure and mechanical properties of aluminum and its alloys has attracted many research efforts. Various alloys, for example, Al-Zr-Sc based alloys [9], AA5052 [10], AA3104 [11], AA7050 [12], AA6111 [13], have been extensively studied. In these works, before cryorolling, the alloys were firstly solution treated at high temperature and then water quenched, followed by low temperature annealing and/or ageing treatments. Under optimal processing conditions, ultrafine grained microstructures with improved tensile strength and good ductility were obtained. Naturally, the improved combination of good mechanical properties are due to reduced density of defects such as dislocation and pronounced precipitation hardening during aging or annealing treatment. Because of the competitive advantage, cryorolling was also used in processing other metals such as titanium [14], magnesium [15] et al. Dramatically, in present work, cryorolling has been successfully adopted to produce UFG structure in an AA6082 alloy extrusion.

In the last year, lots of works have been proposed to improve the work hardening ability of UFG materials. One of typical strategies is to introduce a bi-model or multi-model structure (collectively called hierarchical microstructure) composed of a mixture of micro-sized grains and nano/ultrafine grains, where the micro-sized grains provide large ductility while nano/ultrafine grains offer high strength. In order to obtain hierarchical microstructure, several approaches have been applied. For example, in a study of pure Cu, a non-uniform bimodal grain size distribution was formed by cold rolling together with followed annealing [16], in the obtained material, the fine grains arised from severe deformation and the coarser grains were formed by recrystallization during warm. In other reports, An Al-7Mg alloy was processed by room temperature ECAP and inter-pass annealing, the bimodal microstructure developed was due to the high level of Mg in solid solution, which greatly depressed dynamic

recovery, rearranging dislocation boundaries into regular sub-grain boundaries during annealing [17]. However, in practice, it is may be very difficult to control thermal treatment when one is trying to achieve target grain size and the ways of grain growth due to numbers of uncertainties during processing progress. Interestingly, in our previous work on an AA6060 alloy [18], where by tensioning at 77 K, the surface of the alloy featured that numbers of scattered slip lines formed in some grains but other grains were slip-free, indicating inhomogeneous deformation in material. Thus, it is reasonable to presume that hierarchical microstructure could be obtained if a large deformation strain was carried out at low temperature by cryogenic technique, for example, cryorolling. This is the initial motivation of present work.

As far as we know, cryorolling with the starting materials in the peak-aged state has so far not been reported for heat-treatable aluminum alloys in open literatures. Such processing conditions may require higher rolling forces and the ductility after cryorolling might be reduced. There is also a possibility that the material becomes non-responsive to artificial aging after cryorolling, since the precipitates have already formed prior to the deformation process. Such considerations could be the reason why cryorolling has not been undertaken for initial peak-aged materials.. However, since the aluminum 6000- and 7000 series are precipitation hardenable, the precipitates suppress dynamic recovery during processing, especially at liquid nitrogen temperature [8]. Therefore, it is reasonable to presume that cryorolling in the peak-aged state, could further improve mechanical properties such as strength and hardness. If the above presumption of hierarchical microstructure was justifiable in a cryorolled material, it will be of great significance to develop a simple procedure which can increase strength obviously together with a desirable ductility of the material based on existing industrial techniques. More importantly, the changes in mechanical properties of deformed alloys should be monotonic and thus predictable if an

annealing treatment was conducted, these processes therefore facilitate kinds of requirements for different engineering applications.

In the present work, a peak-aged AA6082 extrusion alloy, which is a relaxed constrained crystal plasticity system, were cryorolled to different thickness reductions. Subsequently, the evolution of microstructure and mechanical properties were carefully analyzed. The mechanisms behind these properties were interpreted based on observations from electron microscopy, e.g. TEM and electron backscattered diffraction (EBSD) in the SEM. The overall purpose of the present work is to evaluate the potential of increasing the strength while maintaining ductility of the peak-aged AA6082 extrusion just using a single procedure, i.e., cryorolling.

2. Experiments

The extruded AA6082 flat profiles, i.e., having 10 mm thickness and 80 mm width, were provided by Hydro Aluminum. The chemical composition is given in Table 1. The profiles went through the following production steps before they were received: First, an as-casted billet was homogenized at 580 °C for 3 hours. Then extrusion was performed at 500 °C with an extrusion ratio of 12, i.e., the average accumulated strain was ~2.5. Immediately after extrusion, the material was quenched in cold water. A subsequent heat treatment conducted at 185 °C for 6 hours put the profiles into the peak-aged condition (T6 temper). The latter constituted the starting material condition for the present investigation, and was denoted as the 0% deformed condition. Rectangular pieces of 40 mm width (along the transverse direction, TD) and 100 mm length (along the extrusion direction, ED) were sawed from the flat profiles for subsequent cryorolling. During the latter process, the rolling direction (RD) was parallel with the previous ED, while the normal direction (ND) was the same. The diameter of the rolls was 200 mm and the rolling speed was 20 rpm. Three reductions were collected for further investigations. These constituted the total thickness

reductions 21%, 42% and 85%, labelled as CR21%, CR42% and CR85%, respectively. These reductions correspond to true strain of 0.23, 0.54 and 1.89. Multiple passes having an approximate 5% reduction each pass achieved these total strains. After each pass, the sheets were kept in liquid nitrogen for 15 min before the subsequent rolling pass was conducted. For comparison, rolling at room temperature (RT) was also performed to an 85% thickness reduction. The deformed structure, texture and mechanical properties of the room temperature rolled condition (RTR85%) were then compared to the corresponding observations achieved with the cryorolled material conditions.

Electron backscatter diffraction (EBSD) was performed in the plane defined by the extrusion (rolling) - normal directions in a Hitachi SU-6600 field emission gun SEM (FEG-SEM) equipped with a Nordif EBSD detector and TSL OIM software. The samples for EBSD characterization were prepared by standard metallographic techniques, followed by electro-chemical polishing (solution of 80% C2H5OH + 20% $HCLO_4$, 20 V, 1.5 A, -30 °C and 15 s). Areas of ~ 1 mm^2 were selected for EBSD analysis of the conditions 0%, CR21% and CR42% using a step size of 2 μm. However, for the conditions CR85% and RTR85% a smaller area of ~ 0.1 mm^2 were scanned and then with a step size of 0.5 μm. Moreover, more detailed EBSD scans were performed for the 42% and 85% CR samples, using a step size of 0.1 μm and 0.05 μm, respectively. The latter scans revealed microstructural details of the most deformed conditions, i.e. expected to contain more fine-scaled items. The the orientation distribution function (ODF) data was generated based on all the scanned points of the respective conditions by the series expansion method with $l_{\max} = 22$ and $\psi_0 = 5^{\circ}$ and orthotropic sample symmetry was adopted.

Transmission electron microscope (TEM) characterization was carried out in a TECHNAI 20G2-S-TWIN TEM using an operating voltage of 200 kV. The TEM foils were prepared by grinding to a thickness of ~200μm, then punching 3 mm diameter disks, and

finally thinning using a Struers twinjet Tenupol-5 electropolisher until perforation. The electro-polishing solution, consisting of 5% perchloric acid, 35% butanol, and 60% methanol and the electrolyte was kept at a constant temperature of -30°C. The voltage utilized was 40V.

Hardness measurements were carried out using Vickers hardness method with 1 kg load. For more reliable results, at least 15 measurements were performed on each rolled alloy.

Parallel to hardness measurement, tensile tests were conducted at room temperature to evaluate the strength and ductility of the various rolled conditions. The specimens were machined from the rolled sheets parallel to the rolling direction having a 50mm gauge length and thickness given by the rolling reduction. A MTS810 servo-hydraulic testing machine was used at a constant crosshead speed, i.e., corresponding to an initial loading rate of 1×10^{-4} s^{-1}. Finally, fractured surfaces of all tensile sample conditions were carefully examined by SEM.

3. Results

3.1. Microband formation and grain subdivision

The EBSD micrographs of the 0%, CR21%, CR42%, CR85% samples are shown in Fig. 1. For comparison, the microstructure of a sample with 85% reduction at room temperature (RTR85%) was also included. The shown micrographs were taken in the ED (RD)-ND plane. The different color contrasts in the EBSD maps correspond to different grain orientations. The black points are non-indexed or with a confidence index (CI) < 0.1. Black and grey lines indicate locations of high angle grain boundaries (HAGBs, $\geqslant$15°) and low angle grain boundaries (LAGBs, 2-15°), respectively. As shown, the starting material (0%) exhibits fibrous grains structure lying along ED (RD), seldom LAGB-free grains could be found (Fig. 1a). With increasing rolling strain (CR21%), the grain are further elongated in the rolling direction. In addition, evidence for crystallographic alignment of microband traces with the slip planes having angle of around 45° to the rolling direction has been presented

(indicated by the black dished lines in Fig. 1b) in some red grains with orientation close to (100). While in the green grains, no traces are visible. Similar results were reported in a study of Al 1575C alloy [19], where deformation bands were visible within a very limited number of grains after tension at 77 K. At the strain increased to high strain of 42%, numbers of microbands formed in the view area (Fig. 1c). Comparing to CR21% sample, obscure microbands can be observed in some half green grains in addition to those in red grains in the CR42% sample, suggesting formation of microband in the alloy volume depends on thickness reduction and more importantly, grain orientations. When the thickness reduction further increases to 85%, one can find that elongated fibrous grains have been fragmented and small equiaxed grains formed (Fig.1d). These equiaxed grains have a wide distribution of grain size ranging from 0.46 μm to 7.85 μm. Moreover, large fraction of non-indexed regions shaded black occupied the viewing area. Generally, these regions arise when patterns are too noisy for the automated band detection and indexing algorithms to work reliably [20]. Please note here a fine step size of 0.05μm has been adopted. Therefore, these regions should be related to fine scale structure and high dislocation density in this highly deformed matrix. While, in case of RTR sample deformed to the same thickness reduction of 85%, little of equiaxed subgrains were observed but instead numbers of elongated subgrains with low aspect ratio dominate due to dynamic recovery at room temperature (Fig. 1e).

A close look at Fig. 1c shows that grain subdivisions occurred in the CR42% sample. Misorientation profiles along directions parallel to the length direction of subdivided grains were measured. Here, two different cases of grains in terms of deformation behavior were selected, i.e. in which (1) high fraction of microband has formed (Line 1), (2) no obvious microbands but just some interrupted slip trace can be observed (Line 2). The corresponding misorientation profile results are shown in Fig. 2. Obviously, the misorientation profile labeled by L1 in Fig. 1c revealed a feature associated with continuous dynamic

recrystallization (CDRX), i.e., proceeded by continuous accumulation of dislocations in microband and eventually resulting in the formation of new grains bounded by HAGBs, which generally are referred to as geometrically necessary boundaries (GNBs) after a lot of studies. Along L1, the maximum point to origin misorientation in this grain is measured to around 22° (red curve in Fig. 2a). This large accumulated misorientation gradient indicates the possibility of formation of HAGB. In fact, several HAGBs already had formed, i.e., the point to point misorientation crossing microbands were already larger than 15° (black curve in Fig. 2a). Therefore HAGBs formed and transformation of band-like subgrains into micro-sized grains with further deformation strain is likely, as evidenced by Fig. 1d. While for the grains coded by green, along L2, both of point to point and point to origin misorientation are much smaller even if measuring distance along L2 is longer than L1, there is no evidence of grain subdivision. These results concluded that the deformed materials produced a heterogeneous volume structure in terms of grain subdivision. The detailed illustrations of related results are given as follows.

The SEM/EBSD technique provides Kernel average misorientation (KAM) as an appropriate parameter to estimate the strain distribution for a given point [21]. For the present image Fig. 3a, the KAM is set for a given point as the numerical average misorientation of that point with all of its three neighbors, the color indicates local misorientation, the largest and lowest local misorientations were indicated by the brightest red and dark blue regions, respectively. It is observed that the highly misoriented regions are consistent with the locations of microband when compared to the EBSD morphology in Fig.1c. Importantly, one can see that the microbands were distributed inhomogeneously cross the view area (Fig. 3a), i.e., some grains have high density of microbands while others are likely microbands-free. This result indicates that different grains respond differently to the same applied load. It is reasonable to suggest that these facts are directly associated with the intrinsic slip

deformation of grains, or more exactly, activation of slip systems at cryogenic temperature, which follows Schmid' law [22].

The Schmid law, given as $\sigma_{0.2} = (1/m)\ \tau_{CRSS}$, where $\sigma_{0.2}$ is the yield strength, τ_{CRSS} is the critical resolved shear stress (CRSS) of a certain deformation behavior in a single crystal, describing that yielding in a single crystal begins when the resolved shear stress on the slip plane along the slip direction exceeds a critical value. As an important parameter, the Schmid factor (SF, m value) is frequently applied to analyze the possibility of the activation of deformation modes with different CRSS upon certain stress. It is well accepted that preferential slip systems are those associated with the highest SF. If provided that deformation characteristics of a grain are unaffected by the presence of neighboring grains, value of SF for all slip system can be calculated according to $m = \cos(\Phi)\cos(\lambda)$ [23], where Φ is angle between applied stress and the normal to the slip plane, λ is the angle between applied stress and the slip direction. Here, it is necessary to note that the present AA6082 alloy has a fibrous structure, presenting a relaxed constrained system, therefore, all grains should be deformed independently under compression stress. Fig 3b is a map of calculated maximum SF in the viewing area for the loading stress applied normal to the RD. The map was generated directly by the OIM software. From which, naturally, one can see that a significant difference in distribution of maximum SF for the single grains coded by different colors. However, comparison between Fig 3a and Fig 3b gives a fact that for the grains having high SF, microband formation is highly likely to occur and shear-driven subdivision tends to take place due to the fact that primary slip system is easily activated [24]. Especially, one can find the small grain size combined with high SF have significant positive effect on subdivision of the fibrous grains (marked by white dished frame), probably due to much less stress required for activation of slip along the highest shear direction in contrast to the case of coarser grains in favorable orientation. While, for those grains with low SF, seldom

microbands formed and no subdivisions of grain are visible. The above results indicate inhomogeneous deformation in material volume has been taken place.

In order to investigate more detailed information on formation mechanism of micro-band dependence of SF, two representatives' coarse grains with difference in possibility of microband formation were selected to perform SF calculations. They were marked as G1 and G2 respectively (Fig. 3b), a set of microbands with parallel straight traces were formed in G1 while the G2 is microband free. The corresponding SFs for all slip systems of them are listed in Table 2 and Table 3, respectively. In which systems with SF $\geq$ 0.4 have been highlighted in bold face [25]. It can be seen from Table 2 that, one slip system coding a direction [101] on the planes (-111), has the highest SF. In a study on microstructural evolution in a mild steel [26], it was showed that cross loading led to microband formation in the material and established that microband formation occurs in the slip system with highest SF. In present work, the [101] oriented grains contained self-screening arrays of microbands aligned with highest SF (-111) slip planes, thus, slip would be intensively activated in this slip system. Similar results were obtained in a 2519-87 aluminum alloy impacted by projectile with velocity of 816 m/s [27]. The authors suggested that the induced microbands had inhomogeneous deformation microstructure and characteristics of microbands were dependent on grain orientation, therefore, the microbands should be confined within individual grains. In our study, it is reasonable to outline from Fig. 3 that the microband crystallographic alignment only formed in favorable orientations and has been maintaining to high thickness reduction, e.g., 42%, as early as it formed at small thickness reduction.

Table 3 shows the calculated SF for the grain coded by green (G2), in which no microbands formed. One can find that there are four slip systems having SF $\geq$ 0.4. In this case, dislocations can disperse out of several planar bands through cross-slip and climb. As a result, homogeneous deformation operates on these slip systems simultaneously [28]. It was

reported that homogeneous deformation is associated with large stacking fault energy of metals such as Al and Cu, which tended to have homogeneous deformation by multi-slip mechanism, leading to subsequent changes in texture components [29].

From the results illustrated above, one can conclude that formation of microbands operated by dislocation slips during deformation is closely related to grain orientation, or more accurately, to SF at cryogenic temperature. During cryorolling, all grains were subjected to same stress that tends to elongate them in RD. However, the amount of strain varies in each grain and formation of microbands in certain grains based on SF, which is varies for different grains. Therefore, hierarchical microstructure was induced by the intrinsic slip deformation of grains in the volume of material as stated above (Fig. 1 and 2). It is reasonable to presume that this microstructural features would have significant influence on the mechanical properties, which will be introduced in latter sectors.

The structure and morphology related to the microbands were further investigated in a selected area on ND-RD section of CR42% sample, as shown in Fig. 4, where microbands operating in planes having angle of 30°-60° to the rolling direction, can be observed frequently in the viewing area. For more details, three observations can be notified:

(1) Grain boundary serrations act as precursor to microbands formation, as shown by red dashed circles in Fig. 4a. This is because microband is a relaxation structure, favorably arising from intense, highly localized area of dislocations [30].

(2) Coexistence of LAGB and HAGB along same microband (the inset picture in Fig. 4a), indicating transformation process of LAGB into HAGB. This is because dislocations in microband can keep continuously rearranging themselves during deformation and misorientation angle across microband increased with strain [31].

(3) The cumulative misorientation profiles along the arrow L3 and L4 on each side of microband evidence that a considerable misorientation gradient exists (Fig. 4c). Also, the

corresponding crystal orientations on each side of the microband are non-symmetric (Fig. 4b). This can be considered as a result of rolling geometrical conditions.

The relative position between neighboring microbands gives rise to grain size while the non-symmetric crystal orientation on each side produces high misorientation across microbands. According to [32], the rotation of lattice close to boundary serrations is more favorable for accommodating deformation, leading to misorientation gradient in lattice under stress field (Fig. 4c). Moreover, due to irregular grain shape, rotation path of lattice should be different on both sides of microband, as a result, the boundaries across microband become high-angled.

3.2 Texture evolution after rolling

The different crystallographic textures evolve in Al alloys depending on thickness reduction. The texture characteristic of AA6082 aluminum alloy, i.e., starting material and cryorolled samples with different thickness reductions, are shown in Fig. 5. The EBSD data were collected from large scanning areas and the corresponding orientation distribution functions (ODF) were calculated. For the 0% material, it is evident of having β-fiber which extends from the brass orientation to the copper orientation through S orientation. The fiber texture may be due to the presence of partly recrystallized grain structures arising from extruded condition and chemical elements of this alloy. Survey of texture map from Fig. 5 is summarized in Fig. 6. The 0% material shows a strong Bs{011}<211> of 23.1 mrd, a significant cube{001}<100> of 18.5 mrd and S{123}<634> of 16.7 mrd, while weak Cu{112}<111> with density of 7.5 mrd. After 21% cryorolling reduction, all orientation density decreased compared to that of 0% material, Bs of 11.4 mrd, cube of 12.9 mrd, S of 9.0 mrd and copper of 5.1 mrd. At thickness reduction of 42%, the intensity of all components was further reduced. The present investigation is matching with the existing literature on a cryorolled Al7075 alloy [33]. The CR85% sample exhibits weakened texture

components of cube with 0.7 mrd, a bit higher Bs with 11.6 mrd, S with 6.0 mrd and copper with 3.1 mrd. The decreased density of each component in the CR85% sample is probably due to the presence of regions with no index patterns (Fig. 1d). For the RTR85% alloy most of texture components have higher density compared to CR alloys such as CR42% sample, suggesting that the progressive weakening of texture is not as significant as that deformed at cryogenic temperature due to activation of slip systems.

As stated above, with the increasing percentage of thickness reduction, the cryorolled alloys showed decreasing density of texture components. The results can be attributed to the accumulation of higher dislocation density and fragmentation of grains caused by the induced strain. As dynamic recovery was suppressed during cryorolling, the accumulated dislocation density tends to rearrange themselves and form cells structure [33], in turn cell substructures can weaken texture [34]. Therefore, mechanical properties would be improved due to low anisotropy in material.

3.3 TEM microstructure of cryorolled materials

Note that high quality EBSD orientation maps can be obtained in the regions containing relative large grains, while the regions with no index patterns probably are predominated by ultrafine grains or disordered lattices. To obtain detailed information of microstructure of these regions, TEM observations were carried out and corresponding micrographs are shown in Fig. 7 and 8. Some typical structures can be observed in these two figures. Fig. 7a and Fig. 7b show evidences of microband, which is a double-dislocation wall structure, emanating from a grain boundary serration and a grain boundary in CR21% and CR42% sample, respectively. This is because these sites can provide dislocation sources for activation of slip system, subsequently, the dislocation walls of a microband can be built up. In addition, Fig. 7b shows characteristic step was formed on the boundary, indicating large shear strains due to localized slip associated with microbands.

Regions of lattice distortion are observed in the grain interior of CR21% sample (Fig. 7a'), possibly caused by second-phase particles [35]. They are usually attributed to a high dislocation density close to grain boundaries featuring their high energy and long-range internal stress [36]. In addition, the dislocation cells having tangled dislocation boundaries were observed in Fig. 7b' in the CR42% sample. The formation of dislocation cells effectively reduces the total energy stored in deformed crystals. Similar observations were also made by Panigrahi et al [37] in a 6063 Al alloy rolled at liquid nitrogen temperature to a true strain of 2.3. They reported that cryorolled samples exhibited heavily deformed grains containing dislocation tangling zones and dense dislocation walls with diffused, non-equilibrium boundaries. Normally, the tangled dislocations which form cells are the relaxed configurations arising from the uniform dislocation microstructure that is the direct results of homogeneous deformation [38]. In present study, as illustrated above, homogeneous deformation is closely related to crystallographic conditions, i.e., in the grains with low SF. As such, several slip systems are activated simultaneously because of nearly equally resolved stresses. Consequently, cells were formed in the alloy (Fig. 7b').

TEM was also performed on the CR85% sample. Fig. 8a shows both ultrafine grains with size of 100-200 nm and nano-grains having size of ~50 nm appeared in the matrix. In addition, micro-sized grains are visible. The ultrafine and nano-grains generally show darker contrast when compared to the micro-sized grains due to the fact that finer grain size allows for stochastically oriented grains, hence, leading to variations in dynamical diffracting conditions [39]. It is also evidenced that thickness extinction contours of ultrafine grains have a strong spread, indicating a high level of internal stress and elastic distortions in crystal lattice. Moreover, a typical dislocation cell structure with size of about 200 nm can be observed in Fig. 8b due to homogeneous deformation.

The average grain sizes in the cryorolled alloys are plotted with the thickness reduction as shown in Fig. 9. One can see that cryorolling introduced a significant decrease in average grain size and moreover, the decrease with further thickness reduction was much slower. The latter indicates dislocation accumulation becomes less pronounced as strain increases. Compared to that of RTR85%, the average grain size of CR85% is lower, which is due to fragmentation of grains deformed at cryogenic temperature.

The hierarchical structure mentioned above can be further evidenced by (sub) grain size distribution, as exemplified by CR85% sample (Fig. 10). Because EBSD maps can only be obtained in areas containing coarse grains, while areas consisting predominantly of ultrafine grains gave no index patterns (Fig. 1d). Here, grain size distribution in number fraction extracted from TEM images is also included. It is revealed that the grain size distribution of CR85% is ranging from 50 nm to 7.8 μm, which is wider than that in a bimodal grain structured Al-Mg alloy proposed in [40]. The latter work illustrated that grain size of the alloy had range from 250 nm to 5.5 μm and thus a high ductility and strength was achieved simultaneously.

3.4. Mechanical properties

The tensile engineering and true stress-strain curves of AA6082 alloy cryorolled at different thickness reduction are shown in Fig. 11a and c, respectively. For comparison, the tensile stress-strain curve of a sample rolled at room temperature to reduction of 85% is also included. The mechanical properties obtained from Fig. 11a were summarized in Fig 11b. One can see that the yield strength of rolled samples has gradually increased as increasing thickness reduction, i.e., the initial material exhibits moderate yield strength (σ_{ys}) of 329 MPa. Afterwards, a significant strength improvement was achieved in the CR21%, CR42% and CR85% sample with corresponding σ_{ys} of 385 MPa, 400 MPa, and 453 MPa, respectively. One can find the last one is much higher than a value of 429 MPa for its counterpart

RTR85%. This result is consistent with the change in hardness as shown in Fig. 9. Generally, the enhancement for tensile strength of AA6082 alloy after cryorolling is due to the fact that cryogenic temperature can effectively suppress dynamic recovery and build up a higher dislocation density in the CR samples, as a result, dislocation motion is severely hindered in highly dislocated matrix during the followed tensile tests, leading to increased strength. Similar results have been reported in Ti-Mo alloy [41], AA5052 alloy [42] et al.

It is very interesting to note the elongation of different samples changes with thickness reductions in an unusual way: the 0% material shows consistent work hardening throughout deformation and achieves an excellent uniform elongation (eu) of 10.2% to failure. The CR21% shows a minor work hardening behavior combined with a decreased eu of 2.3% before necking (Fig. 11a and d). The flow curves of both CR42% and RTR85% sample display different shape compared to others, i.e., both the curves show a very limited uniform elongation (1.7% and 1.6%, respectively) together with strain-softening phenomenon. However, for the CR85% sample, an obvious work hardening characteristic can be observed and a much larger eu of 3.2% is obtained in comparison with CR21%, CR42% and RTR85% samples (Fig. 11b). Along with the improvement of strength as stated above, it is believed this significant enhancement in elongation should be very attractive for further study.

3.5. Fracture characteristics

Fig. 12 shows the scanning electron microscopy (SEM) fractographs of starting material and rolled specimens with different thickness reduction. One can see that all the fractographs consist of well-developed dimples on the surface. For the 0% material, the surface reveals well developed large dimples, which indicates ductile mode facture and thus high tensile elongation. This ductile fracture is supposed to be tearing of metal accompanied by considerable plastic deformation. Fig. 12b and c show that dimples formed in the CR21% and CR42% sample are smaller and have a larger density. The formation of fine and denser

dimples may be attributed to nucleation of a larger number of micro-voids arised from severe strain induced during deformation by cryorolling. For the CR85% sample, numbers of fine dimples can be observed, which can be attributed to the grain refinement, the fine dimples was usually observed in samples subjected to severe plastic deformation (SPD) as reported in the earlier literature [43, 44]. Fig. 12e shows laminated dimples on the fracture of RTR85% sample, indicating the fact that recrystallization did not occur during room temperature rolling. This result is in good agreement with the examination in Fig. 1.

4. Discussion

4.1. Formation of hierarchical microstructure

From geometrical point of view, the model of microbands formation can be depicted in Fig. 13. Fig. 13a displays the color coded KAM map of CR42% sample with forth neighbor misorientation averaging. One can observe that two families of microbands intersect with an angle of 70 degree in some selected areas. This intersection angle follows the crystallography of FCC crystals, where there is an angle of 70.53 degree between {111}. The intersection structures produce micro-sized grains with a low internal dislocation density together with frequently highly dislocated areas. The former is featuring by misorientation of ~4° across the GNBs as shown in Fig. 13b, while the latter should be highly associated with the formation of UFG structure.

Fig. 13c-e shows perspective sketch of microband characteristic and successive stages of micro-sized grains together with ultrafine grains formation with thickness reduction. This sketch map depends on frequent double cross-slip proposed by Chen [45] to produce dislocation sheets consisting of many dipoles of positive Burgers vectors so that dislocation density between the sheets is almost zero (Fig. 13c), which can be evidenced by TEM observation as shown in Fig. 7 a and b. This is because as soon as microbands initialed at

sites such as grain boundaries or other defects, the slip event of slip system with maximum Schmid factor operates. Thereafter, the microbands gradually grow by removal of dislocations sheet 1 to its counterpart sheet 2 who has opposite sign. With deformation, crystal lattice rotation within the band takes place, leading to arrangement of dislocations which enables stress relaxation, where in nature oppositely faced dislocations cancel each other, leading to reduced dislocation density between the two sheets (Fig. 7 a and b).

Soon afterwards, changes in thickness reduction resulted in the variation of slip systems between subsequent passes, promoting new family of microband (Fig. 13d) which was intersecting the first family of microbands. As a result, a hierarchical microstructure developed (Fig. 13e). It should be noted that hierarchical microstructure would also start to appear in microband-free grains (Fig. 1c) under further cryorolling process through rotating lattice toward orientation having highest SF. In other words, as soon as lattice in microband-free grains rotate to favorable orientation, slip localization happen, followed by new microband intersection. These illustrations should be reasonable since the micro-sized grains in Fig. 1d must have been undergone repeated intersection in the whole material volume during cryorolling.

As mentioned above, there were mainly two kinds of dislocation microstructure developed in cryorolled AA6082 alloy by TEM and EBSD observation, i.e., microbands and cells. This is because dislocations move and multiply in two types of cooperative manners. The first one is conducted under the conditions of highly localized deformation, leading to non-equilibrium structures. The second one, which is a strong dependence of the total dislocation energy on dislocation arrangements, is achieved by transferring stored energy system into a state of lowest energy. As a result, dislocation cells are produced (Fig. 7 and 8). The observation of cells in present study is in consistence with reported literature in a cryorolled Al 7075 alloy [33]

4.2. Improvement of strength and elongation

In actual production, the strengthening of Al–Mg–Si alloys comes from the β″ precipitates formed during aging treatment, termed artificial aging at 185°C (AA) and natural aging (NA) at room temperature. In present study, before cryorolling, the materials were subjected to peak-age treatment. In this case, the change in mechanical properties after rolling is mainly attributed to dislocation arrangement and grain size distribution, while the effects of ageing and recovery are negligible. The latter was evidenced by the stable hardness of the rolled alloys after long time room storage. Therefore, the yield strength of the rolled alloys increase with increasing thickness reduction due to increased dislocation density, while the decreased elongation of CR21% and CR42% is attributed to (1) hindered dislocation motion in highly dislocated matrix [46] and (2) the established microbands representing heavily strain localization, which have a deleterious effect on the ductility [47].

For the CR85% sample, the hierarchical microstructure consisting of micro-sized grains, ultrafine grains and nano-grains is supposed to be the main reason for the excellent combination of strength and uniform elongation in comparison with CR42% sample. Generally, the strength is enhanced significantly due to the fact that the numbers of grain boundaries can retard dislocation movement, as expected from the Hall-Petch relationship. Meanwhile, the hierarchical grain structure can induce enhanced work hardening that stabilize the tensile deformation to a high uniform elongation [48]. This is because during tensile test, micro-sized grains are effective in storing dislocations, yielding a pronounced strain hardening. In addition, the multimodal size distributions may cause the deformation via complex strain paths rather than localization behavior. As a result, the uniform elongation is sustained to a large strain.

It is necessary to mention that another strategy was adopted in this study. This strategy is based on formation of UFG structure with high volume of HAGBs and the related

non-equilibrium state capable of grain boundary sliding (GBS) [49]. Deformation along grain boundary can be much easier when GBS are present, an indirect evidence of the its important role playing in deformation behavior of UFG materials is the usual observations of strain rate sensitivity (SRS) of flow stress that has been reported in numbers of recent works [50, 51]. Because the UFG alloy was deformed by means of GBS during both cryorolling and tensioning, no localized deformation occurred in the alloy, as exemplified in one typical case (Fig. 1c).

In a short summary, the present work achieved desirable combination of ductility and strength of an extrusion AA6082 alloy having fibrous structure by a simple procedure, i.e., cryorolling. Moreover, the microstructure evolution with thickness reduction was tried to establish. As far as we can judge, this method can be applied to many commercial alloy systems that have relaxed constrained structure. Due to the simplicity, it is reasonable to adopt cryorolling into current industrial processes and exploit its potential for large-scale industrial applications of UFG materials in future.

5. Conclusions

Cryorolling process has been carried out on a peak-aged AA6082 extrusion, the effects of thickness reduction on the microstructural refinement and mechanical properties were investigated. The following conclusions are made:

(1) The deformation induced at cryogenic temperature facilitates the microbands formation in the grains having the highest SF, thereafter, the microbands act as favorable sites for the grain subdivision in the cryorolled alloy. Because grains with various orientations respond differently to the same applied load in terms of activation of slip systems at cryogenic temperature, grain hierarchy consisting of microband accumulation and microband-free was happened in the alloy.

(2) As thickness reduction further increase, intersection between different families of microbands took place, leading to development of hierarchical microstructure having nano-grains, ultrafine grains and micro-sized grains in the alloy, which was evidenced by both EBSD and TEM in the CR85% sample.

(3) During tensile tests, the strength of cryorolled alloy increased with the thickness reduction because of the pre-existed high dislocation density and the increased fraction of grain boundaries. However, the corresponding uniform elongation gradually decreased for the 0%, CR21%, CR42% sample but again increased obviously in the CR85% sample. The formers are related to hindered dislocation motion and established microbands, while the latter is attributed to the hierarchical microstructure.

(4)It was confirmed that the single procedure, i.e. cryorolling, can be used for simultaneously increase the strength and maintain ductility of the peag-aged AA6082 extrusion.

Acknowledgments

This work was supported by the Program for Joint Research Centers between Norway and China at NTNU, Norwegian University of Science and Technology (Pnr. 81730200), and the Key University Science Research Project of Jiangsu Province (Grant No. 14KJA430002). Zebing Xu also thanks Dr. Trond Furu at Hydro Aluminum for providing the experimental materials.

Reference

[1] Q. Wang, Microstructural effects on the tensile and fracture behavior of aluminum casting alloys A356/357, Metallurgical and Materials Transactions A, 34 (2003) 2887-2899.

[2] A.V. Mikhaylovskaya, A.D. Kotov, A.V. Pozdniakov, V.K. Portnoy, A high-strength aluminium-based alloy with advanced superplasticity, Journal of Alloys and Compounds, 599 (2014) 139-144.

[3] S. Gudić, I. Smoljko, M. Kliškić, The effect of small addition of tin and indium on the corrosion behavior of aluminium in chloride solution, Journal of Alloys and Compounds, 505 (2010) 54-63.
[4] A.S. Khan, B. Farrokh, L. Takacs, Effect of grain refinement on mechanical properties of ball-milled bulk aluminum, Materials Science and Engineering: A, 489 (2008) 77-84.
[5] A. Korchef, Y. Champion, N. Njah, X-ray diffraction analysis of aluminium containing Al8Fe2Si processed by equal channel angular pressing, Journal of Alloys and Compounds, 427 (2007) 176-182.
[6] A. Vorhauer, R. Pippan, On the homogeneity of deformation by high pressure torsion, Scripta Materialia, 51 (2004) 921-925.
[7] Y. Li, N. Tao, K. Lu, Microstructural evolution and nanostructure formation in copper during dynamic plastic deformation at cryogenic temperatures, Acta materialia, 56 (2008) 230-241.
[8] N. Naga Krishna, A.K. Akash, K. Sivaprasad, R. Narayanasamy, Studies on void coalescence analysis of nanocrystalline cryorolled commercially pure aluminium formed under different stress conditions, Materials & Design, 31 (2010) 3578-3584.
[9] C. Booth-Morrison, D.C. Dunand, D.N. Seidman, Coarsening resistance at 400 °C of precipitation-strengthened Al–Zr–Sc–Er alloys, Acta materialia, 59 (2011) 7029-7042.
[10] W. Liu, J. Morris, Effect of hot and cold deformation on the β fiber rolling texture in continuous cast AA 5052 aluminum alloy, Scripta Materialia, 52 (2005) 1317-1321.
[11] Q. Liu, Z. Yao, A. Godfrey, W. Liu, Effect of particles on microstructural evolution during cold rolling of the aluminum alloy AA3104, Journal of Alloys and Compounds, 482 (2009) 264-271.
[12] D. Wang, Z. Ma, Z. Gao, Effects of severe cold rolling on tensile properties and stress corrosion cracking of 7050 aluminum alloy, Materials Chemistry and Physics, 117 (2009) 228-233.
[13] S.-B. Kang, B.-K. Min, H.-W. Kim, D.S. Wilkinson, J. Kang, Effect of asymmetric rolling on the texture and mechanical properties of AA6111-aluminum sheet, Metallurgical and Materials Transactions A, 36 (2005) 3141-3149.
[14] S.V. Zherebtsov, G.S. Dyakonov, A.A. Salem, V.I. Sokolenko, G.A. Salishchev, S.L. Semiatin, Formation of nanostructures in commercial-purity titanium via cryorolling, Acta materialia, 61 (2013) 1167-1178.
[15] J. Luo, Y. Yan, J. Zhang, L. Zhuang, Microstructure and mechanical properties of a basal textured AZ31 magnesium alloy cryorolled at liquid-nitrogen temperature, Metals and Materials International, 22 (2016) 637-641.
[16] Y. Wang, M. Chen, F. Zhou, E. Ma, High tensile ductility in a nanostructured metal, Nature, 419 (2002) 912-915.
[17] M. Zha, Y. Li, R.H. Mathiesen, R. Bjørge, H.J. Roven, High ductility bulk nanostructured Al–Mg binary alloy processed by equal channel angular pressing and inter-pass annealing, Scripta Materialia, 105 (2015) 22-25.

[18] Z. Xu, H.J. Roven, Z. Jia, Mechanical properties and surface characteristics of an AA6060 alloy strained in tension at cryogenic and room temperature, Materials Science and Engineering: A, 648 (2015) 350-358.
[19] D. Zhemchuzhnikova, A. Mogucheva, R. Kaibyshev, Mechanical properties and fracture behavior of an Al–Mg–Sc–Zr alloy at ambient and subzero temperatures, Materials Science and Engineering: A, 565 (2013) 132-141.
[20] S.I. Wright, M.M. Nowell, S.P. Lindeman, P.P. Camus, M. De Graef, M.A. Jackson, Introduction and comparison of new EBSD post-processing methodologies, Ultramicroscopy, 159, Part 1 (2015) 81-94.
[21] M. Calcagnotto, D. Ponge, E. Demir, D. Raabe, Orientation gradients and geometrically necessary dislocations in ultrafine grained dual-phase steels studied by 2D and 3D EBSD, Materials Science and Engineering: A, 527 (2010) 2738-2746.
[22] M. Arminjon, A regular form of the Schmid law. Application to the ambiguity problem, Textures and Microstructures, 14 (1991) 1121.
[23] Y.-Q. Wu, H.-J. Shi, K.-S. Zhang, H.-Y. Yeh, Numerical investigation of grain boundary effects on elevated-temperature deformation and fracture, International Journal of Solids and Structures, 43 (2006) 4546-4577.
[24] X. Li, Z. Wang, S. Li, Deformation bands in cyclically deformed copper single crystals, Philosophical Magazine A, 80 (2000) 1901-1912.
[25] A.D. Kammers, J. Wongsa-Ngam, T.G. Langdon, S. Daly, The effect of microstructure heterogeneity on the microscale deformation of ultrafine-grained aluminum, Journal of materials research, 29 (2014) 1664-1674.
[26] S. Thuillier, E.F. Rauch, Development of microbands in mild steel during cross loading, Acta Metallurgica et Materialia, 42 (1994) 1973-1983.
[27] X.-p. Liang, H.-z. Li, L. Huang, T. Hong, B. Ma, Y. Liu, Microstructural evolution of 2519-T87 aluminum alloy obliquely impacted by projectile with velocity of 816 m/s, Transactions of Nonferrous Metals Society of China, 22 (2012) 1270-1279.
[28] A.A. Csontos, E.A. Starke, The effect of inhomogeneous plastic deformation on the ductility and fracture behavior of age hardenable aluminum alloys, International Journal of Plasticity, 21 (2005) 1097-1118.
[29] N. Jia, P. Eisenlohr, F. Roters, D. Raabe, X. Zhao, Orientation dependence of shear banding in face-centered-cubic single crystals, Acta materialia, 60 (2012) 3415-3434.
[30] K. Shen, B.J. Duggan, Microbands and crystal orientation metastability in cold rolled interstitial-free steel, Acta materialia, 55 (2007) 1137-1144.
[31] D. Poddar, P. Cizek, H. Beladi, P.D. Hodgson, Orientation Dependence of the Deformation Microstructure in a Fe-30Ni-Nb Model Austenitic Steel Subjected to Hot Uniaxial Compression, Metallurgical and Materials Transactions A, 46 (2015) 5933-5951.

[32] D.H. Shin, I. Kim, J. Kim, K.-T. Park, Grain refinement mechanism during equal-channel angular pressing of a low-carbon steel, Acta materialia, 49 (2001) 1285-1292.
[33] R. Jayaganthan, H.-G. Brokmeier, B. Schwebke, S. Panigrahi, Microstructure and texture evolution in cryorolled Al 7075 alloy, Journal of Alloys and Compounds, 496 (2010) 183-188.
[34] H.-w. Jiang, N. Li, Z. Xu, Z.-s. Fan, H.-p. Yu, L. Liu, Microstructure, texture and mechanical properties of 5A02 aluminum alloy tubes under electromagnetic bulging, Materials & Design, 82 (2015) 106-113.
[35] B.Q. Han, J.Y. Huang, Y.T. Zhu, E.J. Lavernia, Strain rate dependence of properties of cryomilled bimodal 5083 Al alloys, Acta materialia, 54 (2006) 3015-3024.
[36] G. Nurislamova, X. Sauvage, M. Murashkin, R. Islamgaliev, R. Valiev, Nanostructure and related mechanical properties of an Al–Mg–Si alloy processed by severe plastic deformation, Philosophical Magazine Letters, 88 (2008) 459-466.
[37] S.K. Panigrahi, R. Jayaganthan, Development of ultrafine-grained Al 6063 alloy by cryorolling with the optimized initial heat treatment conditions, Materials & Design, 32 (2011) 2172-2180.
[38] D.H. Shin, J.-J. Park, Y.-S. Kim, K.-T. Park, Constrained groove pressing and its application to grain refinement of aluminum, Materials Science and Engineering: A, 328 (2002) 98-103.
[39] X. Zhang, T. Hu, J.F. Rufner, T.B. LaGrange, G.H. Campbell, E.J. Lavernia, J.M. Schoenung, K. van Benthem, Metal/ceramic interface structures and segregation behavior in aluminum-based composites, Acta materialia, 95 (2015) 254-263.
[40] M. Zha, Y. Li, R.H. Mathiesen, R. Bjørge, H.J. Roven, Achieve high ductility and strength in an Al–Mg alloy by severe plastic deformation combined with inter-pass annealing, Materials Science and Engineering: A, 598 (2014) 141-146.
[41] C.-C. Chung, S.-W. Wang, Y.-C. Chen, C.-P. Ju, J.-H. Chern Lin, Effect of cold rolling on structure and tensile properties of cast Ti–7.5Mo alloy, Materials Science and Engineering: A, 631 (2015) 52-66.
[42] W. Bo, X.-h. Chen, F.-s. Pan, J.-j. Mao, F. Yong, Effects of cold rolling and heat treatment on microstructure and mechanical properties of AA 5052 aluminum alloy, Transactions of Nonferrous Metals Society of China, 25 (2015) 2481-2489.
[43] A. Vinogradov, T. Ishida, K. Kitagawa, V.I. Kopylov, Effect of strain path on structure and mechanical behavior of ultra-fine grain Cu–Cr alloy produced by equal-channel angular pressing, Acta materialia, 53 (2005) 2181-2192.
[44] D.R. Fang, Q.Q. Duan, N.Q. Zhao, J.J. Li, S.D. Wu, Z.F. Zhang, Tensile properties and fracture mechanism of Al–Mg alloy subjected to equal channel angular pressing, Materials Science and Engineering: A, 459 (2007) 137-144.
[45] Q. Chen, A. Ngan, B. Duggan, Microstructure evolution in an interstitial-free steel during cold rolling at low strain levels, in: Proceedings of the Royal Society of London A: Mathematical, Physical and Engineering Sciences, The Royal Society, 2003, pp. 1661-1685.

[46] Y. Xiong, T. He, J. Wang, Y. Lu, L. Chen, F. Ren, Y. Liu, A.A. Volinsky, Cryorolling effect on microstructure and mechanical properties of Fe–25Cr–20Ni austenitic stainless steel, Materials & Design, 88 (2015) 398-405.
[47] X.H. Hu, M. Jain, D.S. Wilkinson, R.K. Mishra, Microstructure-based finite element analysis of strain localization behavior in AA5754 aluminum sheet, Acta materialia, 56 (2008) 3187-3201.
[48] Y. Hailiang, L. Cheng, T. Kiet, L. Xianghua, S. Yong, Y. Qingbo, K. Charlie, Asymmetric cryorolling for fabrication of nanostructural aluminum sheets, Scientific reports, 2 (2012).
[49] N.Q. Chinh, P. Szommer, Z. Horita, T.G. Langdon, Experimental Evidence for Grain-Boundary Sliding in Ultrafine-Grained Aluminum Processed by Severe Plastic Deformation, advanced materials, 18 (2006) 34-39.
[50] J. May, H. Höppel, M. Göken, Strain rate sensitivity of ultrafine-grained aluminium processed by severe plastic deformation, Scripta Materialia, 53 (2005) 189-194.
[51] H. Kolsky, An investigation of the mechanical properties of materials at very high rates of loading, Proceedings of the Physical Society. Section B, 62 (1949) 676.

List of tables

Figure captions

Fig. 6. Orientation density of rolling texture components (Brass, Cube, S, Copper) as a function of thickness reduction.

Fig. 7. (a) Microband growing from a grain boundary kinking in the CR21% sample, (a') pinned dislocations by precipitates and region of lattice distortion in the CR21% sample, the inset confirms that the image is obtained according to a [001] zone axis, (b) microband shearing grain boundary and step formed in the CR42% sample, (b') dislocation cells having tangled dislocation boundaries in the CR42% sample.

Fig. 8. TEM micrographs of CR85% showing (a) hierarchical microstructure featuring a mixture of nano grains, ultrafine grains and micro-sized grains, (b) cell structure with high density of dislocation at the boundary but a quite low density inside.

Fig. 9. Average grain size and hardness of rolled AA6082 alloy as a function of thickness reduction.

Fig. 10. Grain size distribution of the CR85% sample in (a) number fraction extracted from TEM images, and (b) area fraction measured by EBSD maps. The obtained statistics reveal a very wide grain size distribution ranging from 50 nm to 7.8 μm.

Fig. 11. (a) Engineering stress-strain curves of starting material 0% (starting material), CR21%, CR42%, CR85% and RTR85% samples, (b) summarization of yield strength and uniform elongation shown in (a), for viewing convenience, the values of corresponding uniform elongation were displayed, (c) true stress-strain curve and (d) work hardening rate curve as a function of true strain of starting material, CR21%, CR42%, CR85% and RTR85% samples.

Fig. 12. Fractographs of cryorolled (CR) AA6082 alloys with different reduction thickness: (a) 0% (starting material), (b) 22%, (c) 42%, (d) 85%. For comparison, fracture photograph of RTR85% is shown in (e).

Fig. 13. (a) KAM map showing microbands and microbands intersection in the CR42% sample, (b) misorientation profiles measured along red arrow in (a), (c-e) schematic maps showing development of hierarchical microstructure with thickness reduction, where (c) microbands form by arrangement of dislocations of opposite sign between two sheets, (d) two families of microbands intersecting with an

angle of 70 degree, (e) formation of micro-sized grains and ultrafine grains due to intersection of microbands.

Table 2 Chemical composition of the present AA6082 alloy (wt.%).

Si	Fe	Mn	Mg	Zn	Al
1.005	0.165	0.497	0.687	0.01	balance

Table 2 Schmid factors and their relevant importance for various slip systems in G1. The crystallographic plane and the crystallographic direction is (2 3 15), [-24 1 3], respectively.

crystallographic plane (hkl)	crystallographic direction [uvw]	Schmid factor	Order of slip factor
111	01-1	0.21	
111	10-1	0.32	
111	1-10	0.11	
-111	01-1	0.13	
-111	101	0.45	**(1)**
-111	110	0.32	
1-11	011	0.34	
1-11	10-1	0.13	
1-11	110	0.21	
11-1	011	0	
11-1	101	0	
11-1	1-10	0	

Table 3 Schmid factors and their relevant importance for various slip systems in G2. The crystallographic plane and the crystallographic direction is (40 41 1), [1 1 -81], respectively.

crystallographic plane (hkl)	crystallographic direction [uvw]	Schmid factor	Order of slip factor
111	01-1	0.41	**(1)**
111	10-1	0.40	**(1)**
111	1-10	0.01	
-111	01-1	0.01	
-111	101	0.01	
-111	110	0.02	
1-11	011	0	
1-11	10-1	0	
1-11	110	0	
11-1	011	0.42	**(1)**
11-1	101	0.41	**(1)**
11-1	1-10	0.01	

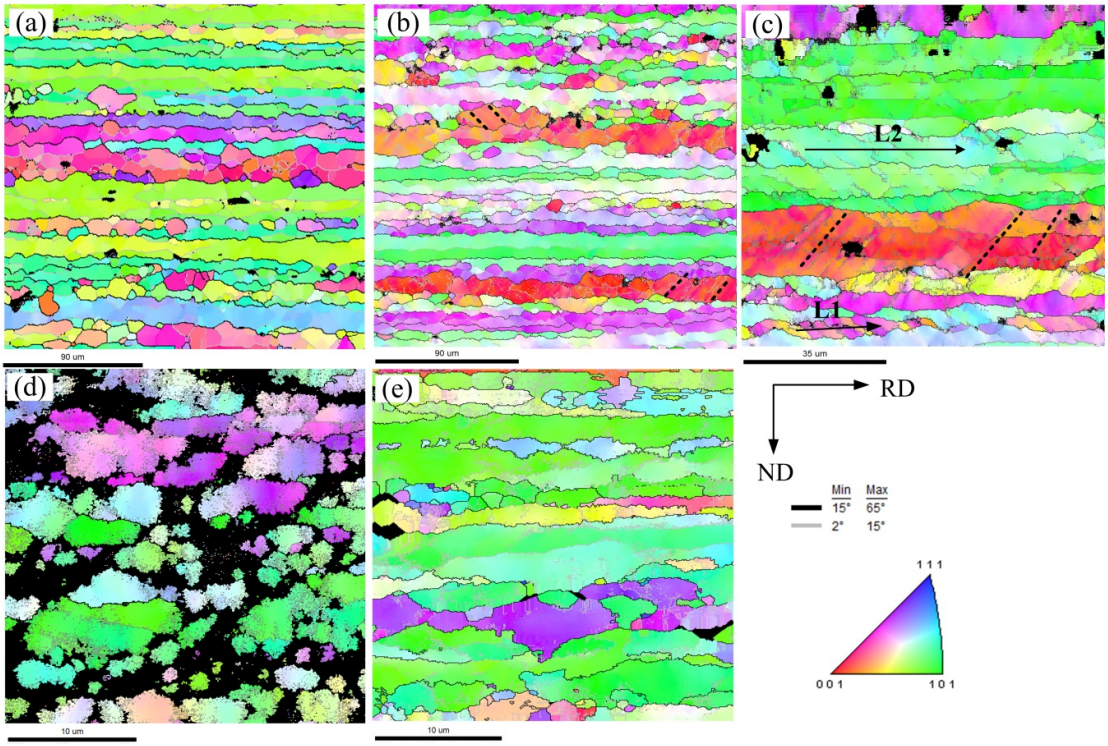

Fig. 1 Typical microstructures in the peak-aged AA6082 alloy after multiple cryorolling to thickness reduction of (a) 0%, (b) 21%, (c) 42%, (d) 85%. For comparison, the microstructure of a sample rolled at room temperature to a thickness reduction of 85% is also included in (e). The grey and black lines correspond to the subgrain/grain boundaries with misorientation of $2° \leq \theta < 15°$ and $15° \leq \theta < 65°$, respectively. The dashed black lines in (b) and (c) represent microbands. The lower right triangle is the color code for the orientation maps.

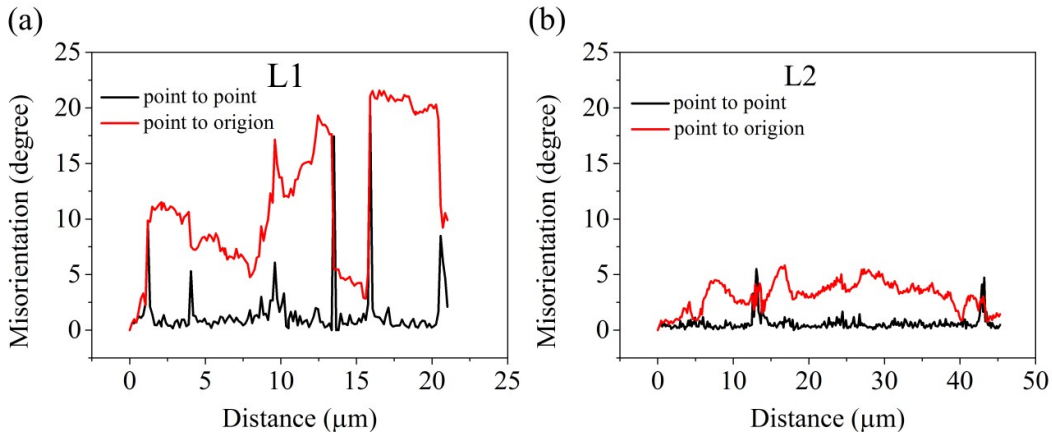

Fig. 2. Misorientation profiles measured along line L1 and L2 in Fig. 1c.

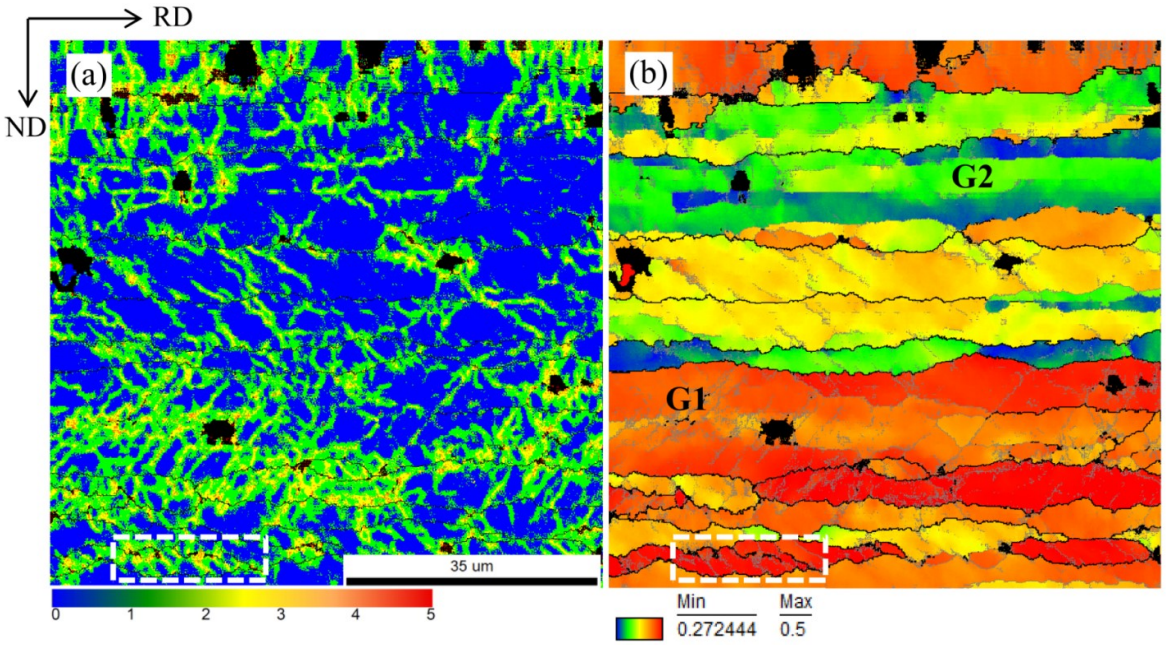

Fig. 3 (a) KAM map showing the local misorientation gradient of the CR42% sample, (b) Schmid factor map of the same area of (a). Two grains G1 and G2 in (b) were selected for Schmid factor calculations. The white dashed frame represents typical subdivision of a small fibrous grain.

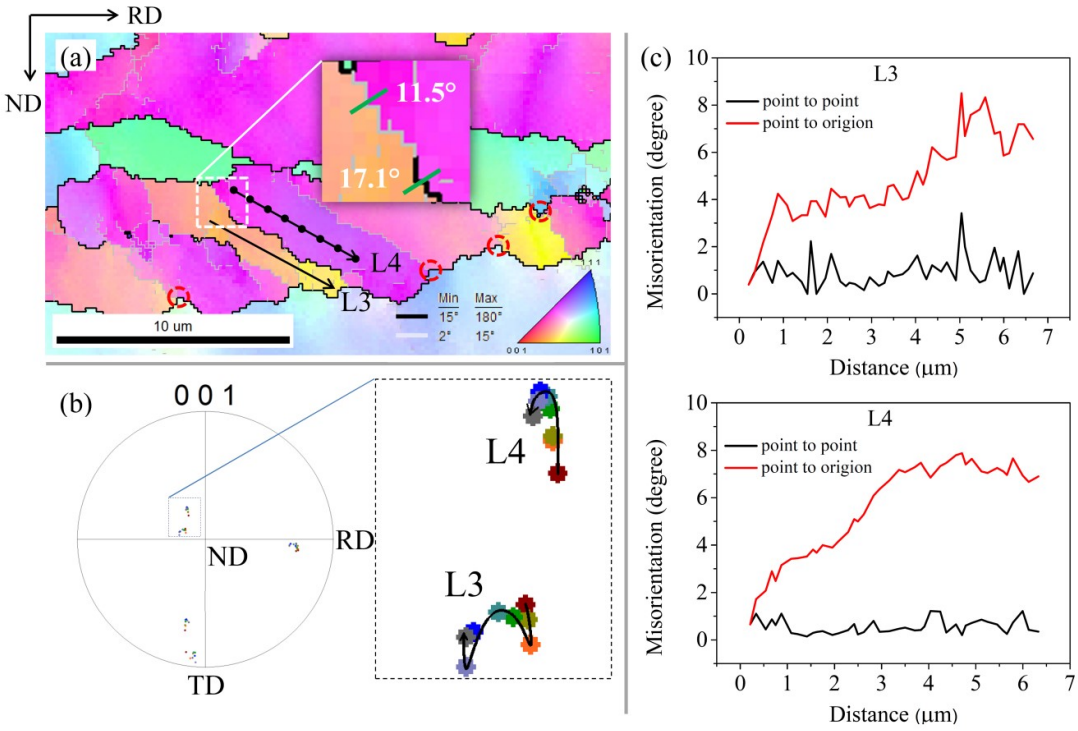

Fig. 4. (a) Orientation map of the CR42% sample, the inset shows LAGB and HAGB coexist in the same boundary, implying the boundary is in the process of transforming from LAGB to HAGB, (b) oriented stereographic projections for the arrow L3 and L4 marked in (a), respectively, (c) cumulative misorientation profiles along the arrow L3 and L4 shown in (a).

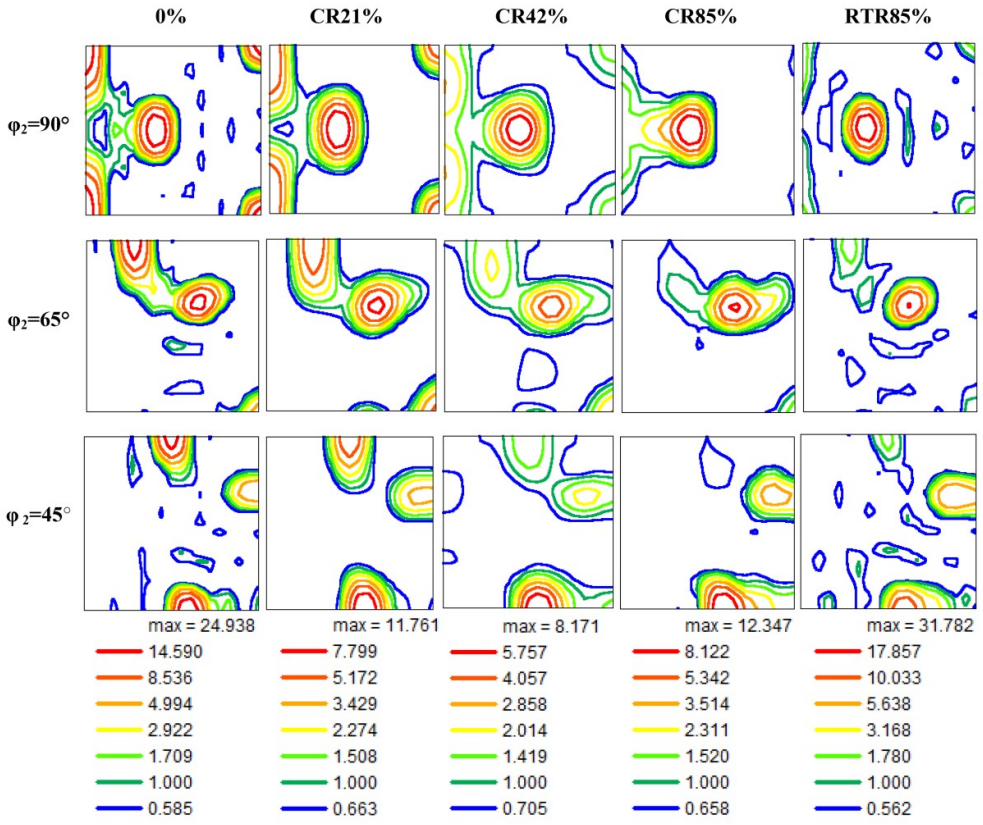

Fig. 5. φ2= 45°, φ2= 65°, φ2= 90° sections of orientation distribution functions measured by EBSD from the ST, CR21%, CR42%, CR85% and RTR85% samples.

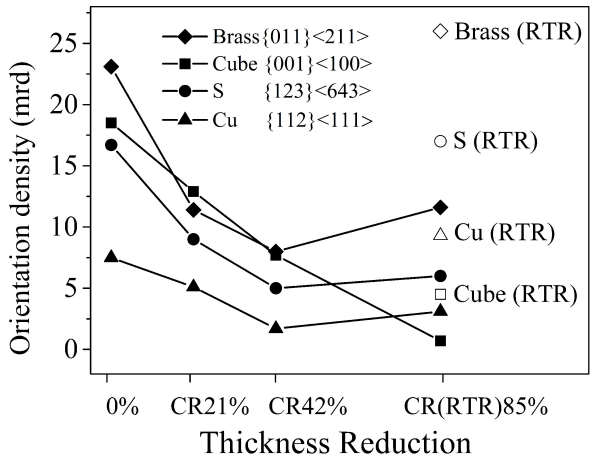

Fig. 6. Orientation density of rolling texture components (Brass, Cube, S, Copper) as a function of thickness reduction.

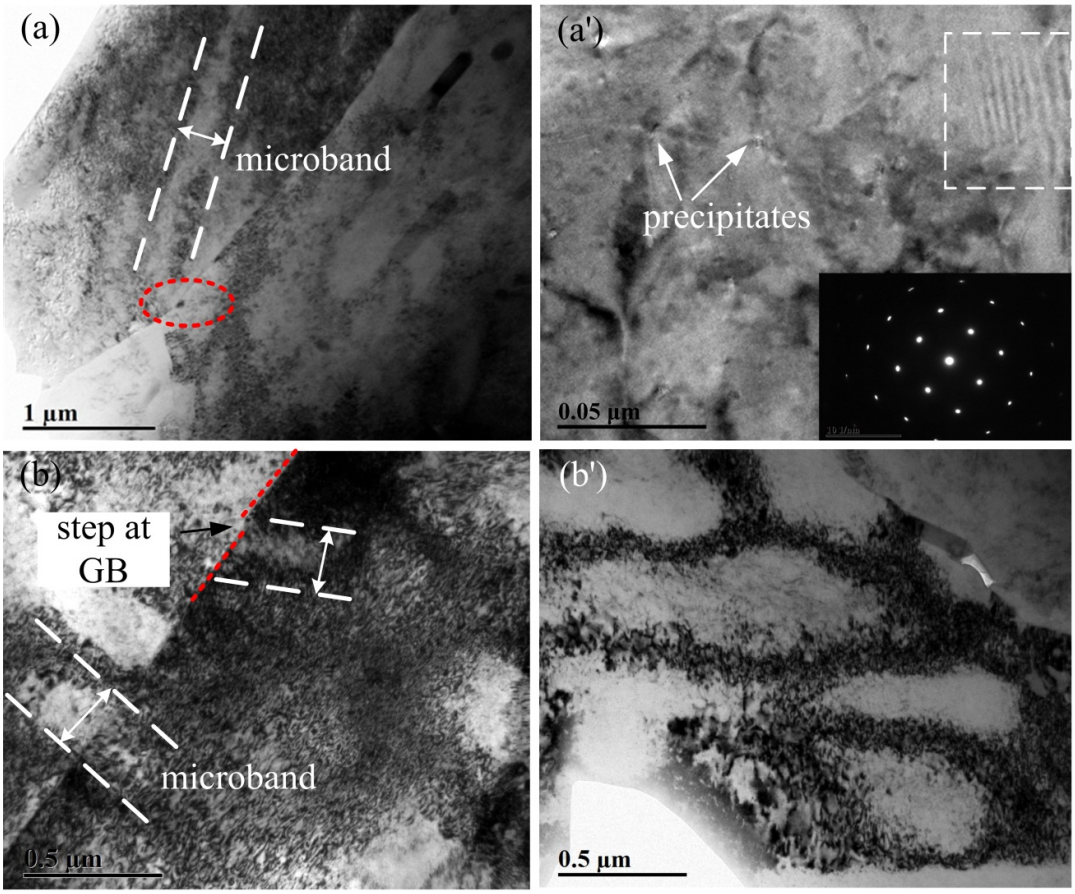

Fig. 7. (a) Microband growing from a grain boundary kinking in the CR21% sample, (a') pinned dislocations by precipitates and region of lattice distortion in the CR21% sample, the inset confirms that the image is obtained according to a [001] zone axis, (b) microband shearing grain boundary and step formed in the CR42% sample, (b') dislocation cells having tangled dislocation boundaries in the CR42% sample.

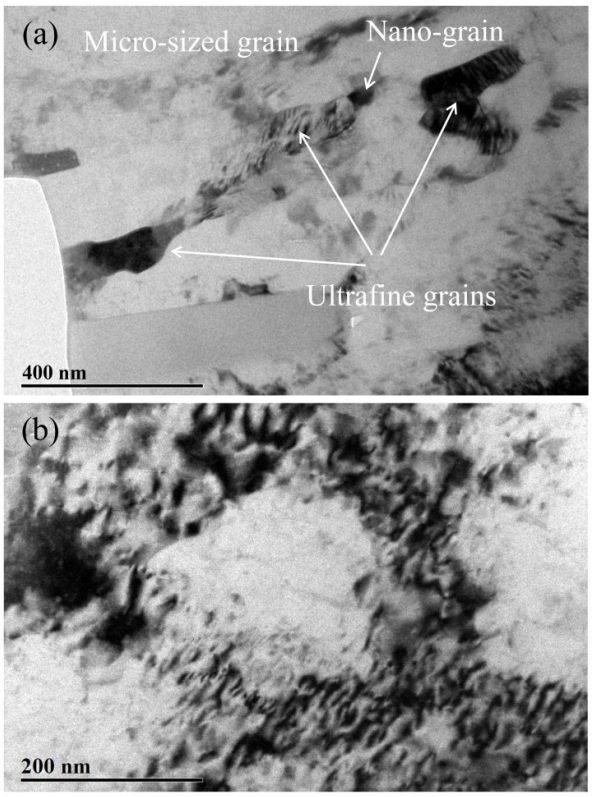

Fig. 8. TEM micrographs of CR85% showing (a) hierarchical microstructure featuring a mixture of nano- grains, ultrafine grains and micro-sized grains, (b) cell structure with high density of dislocation at the boundary but a quite low density inside.

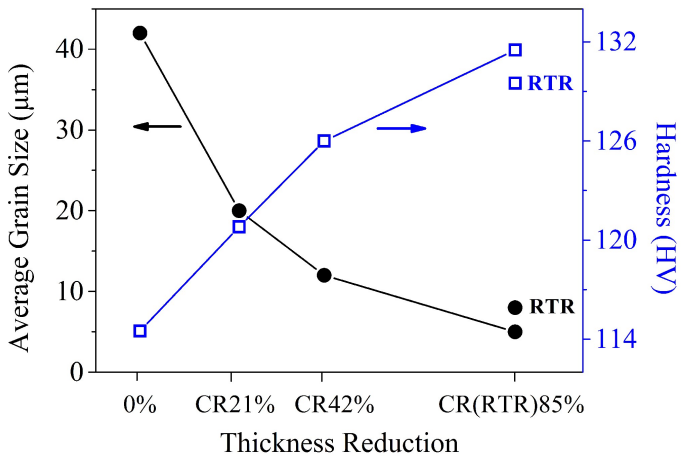

Fig. 9. Average grain size and hardness of rolled AA6082 alloy as a function of thickness reduction.

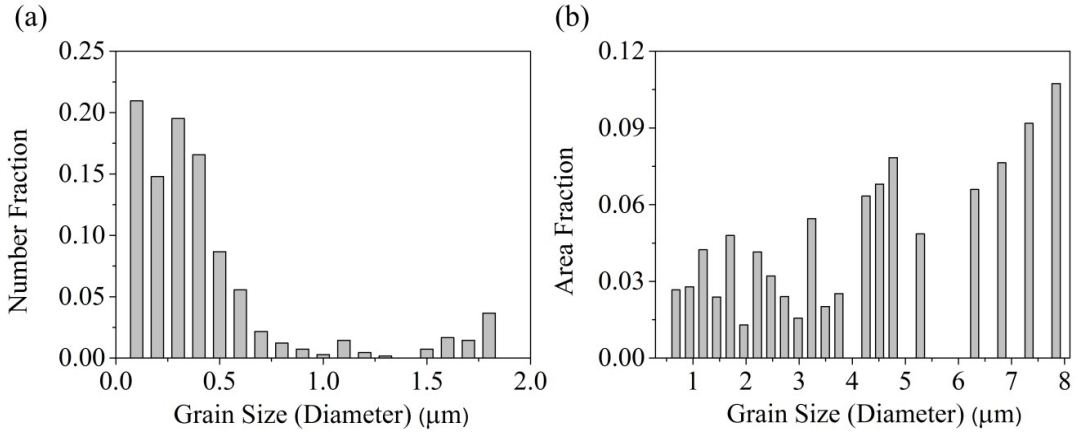

Fig. 10. Grain size distribution of the CR85% sample in (a) number fraction extracted from TEM images, and (b) area fraction measured by EBSD maps. The obtained statistics reveal a very wide grain size distribution ranging from 50 nm to 7.8 μm.

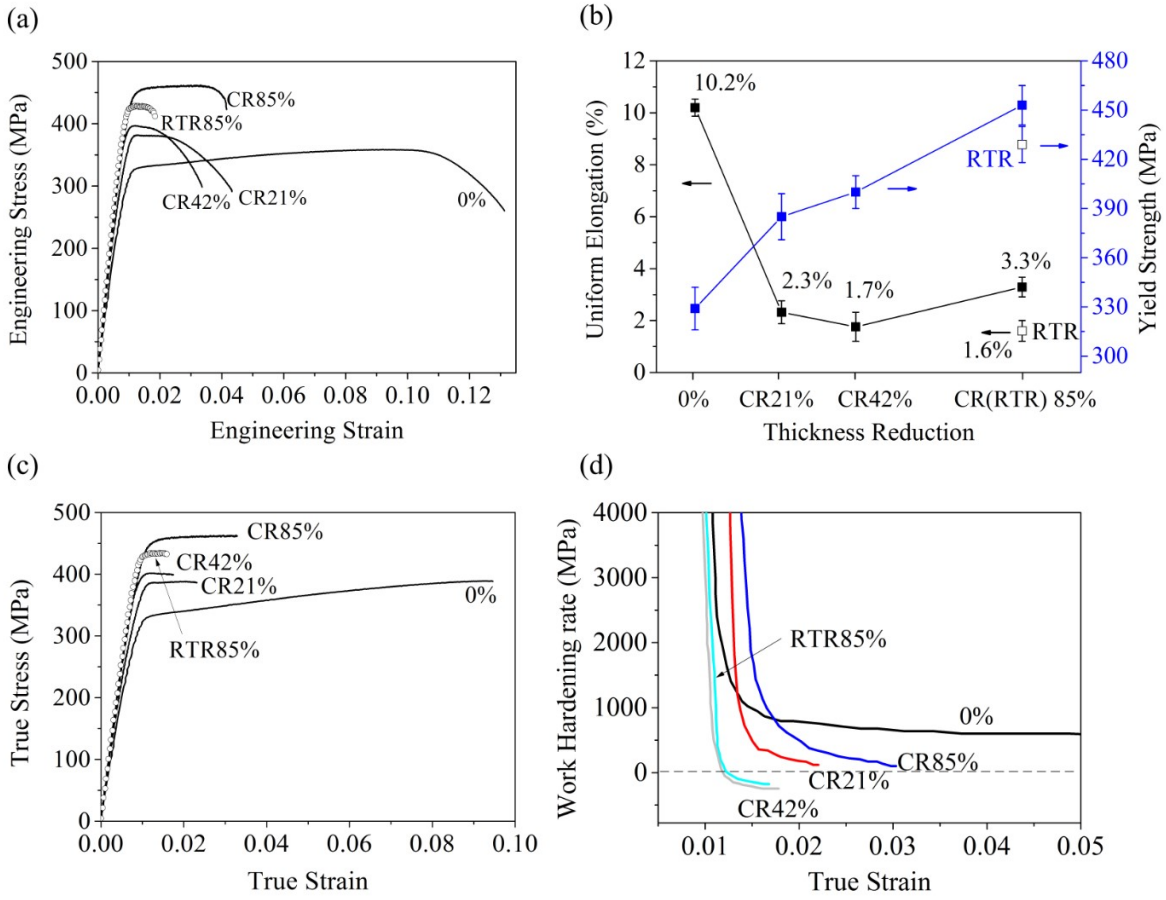

Fig. 11. (a) Engineering stress-strain curves of starting material 0% (starting material), CR21%, CR42%, CR85% and RTR85% samples, (b) summarization of yield strength and uniform elongation shown in (a), for viewing convenience, the values of corresponding uniform elongation were displayed, (c) true stress-strain curve and (d) work hardening rate curve as a function of true strain of starting material, CR21%, CR42%, CR85% and RTR85% samples.

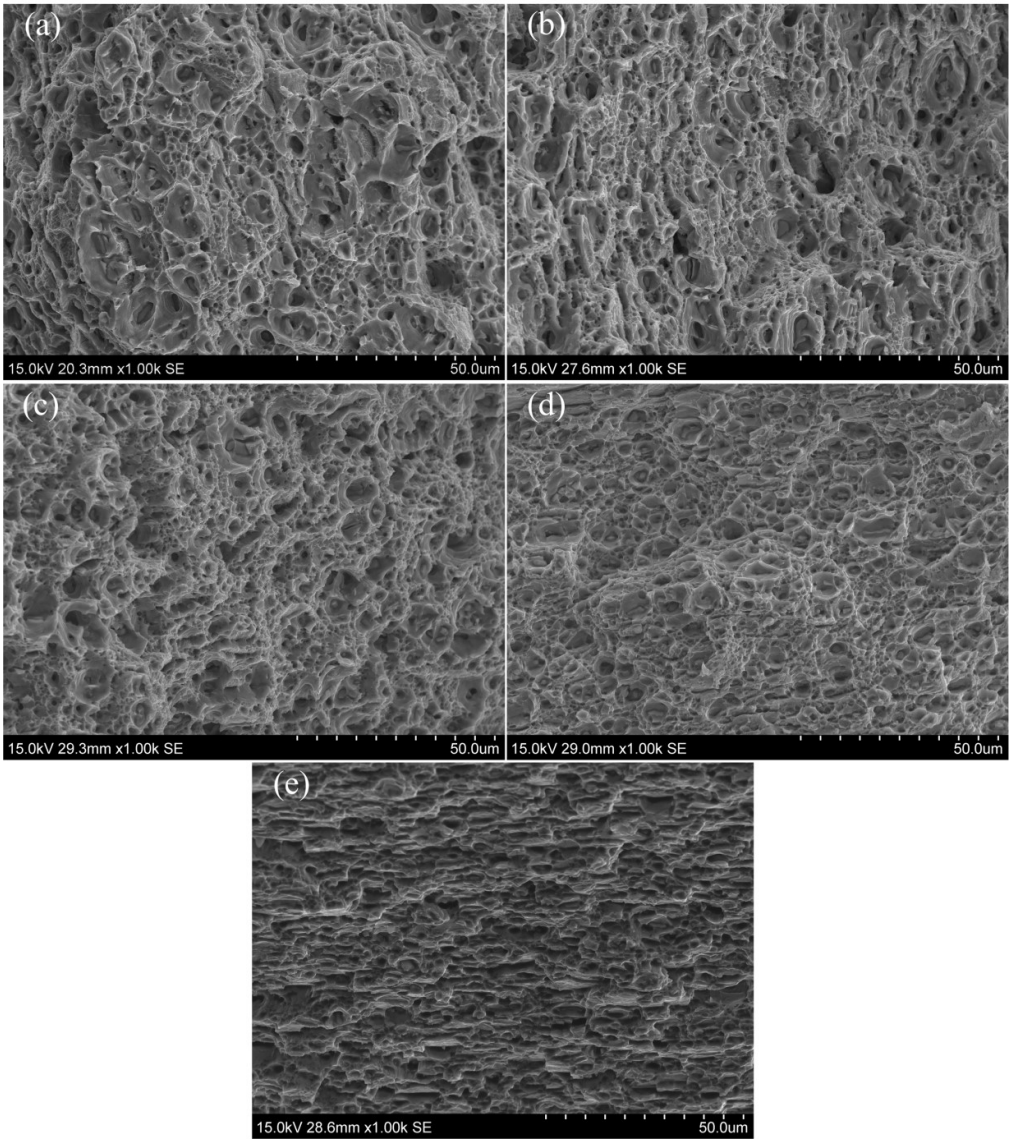

Fig. 12. Fractographs of cryorolled (CR) AA6082 alloys with different reduction thickness: (a) 0% (starting material), (b) 22%, (c) 42%, (d) 85%. For comparison, fracture photograph of RTR85% is shown in (e).

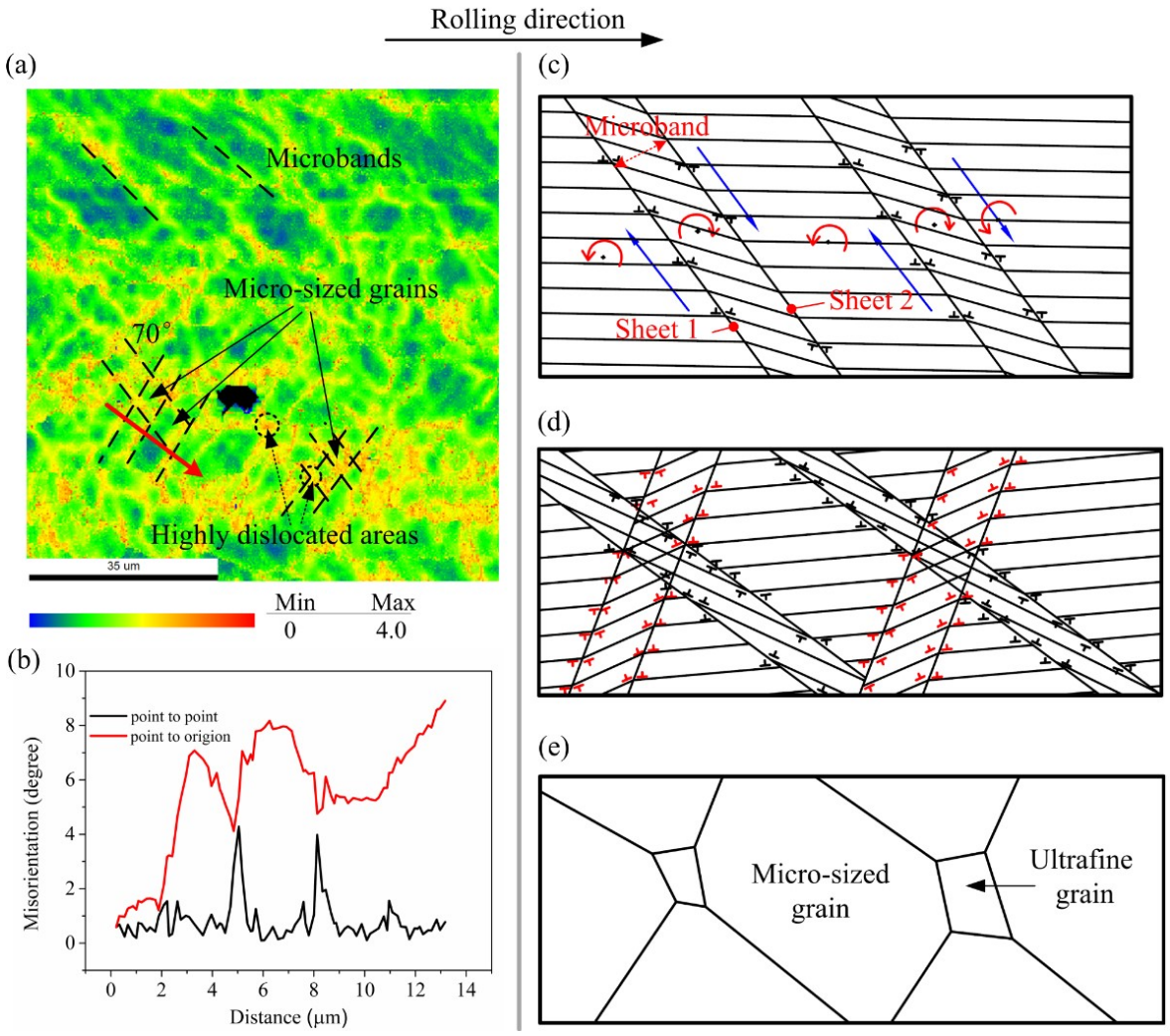

Fig. 13. (a) KAM map showing microbands and microbands intersection in the CR42% sample, (b) misorientation profiles measured along red arrow in (a), (c-e) schematic maps showing development of hierarchical microstructure with thickness reduction, where (c) microbands form by arrangement of dislocations of opposite sign between two sheets, (d) two families of microbands intersecting with an angle of 70 degree, (e) formation of micro-sized grains and ultrafine grains due to intersection of microbands.